

# Composite Stellar Populations and Element by Element Abundances in the Milky Way Bulge and Elliptical Galaxies

Baitian Tang<sup>1\*</sup>, Guy Worthey<sup>1†</sup>, and A. Bianca Davis<sup>2</sup>

<sup>1</sup>*Department of Physics and Astronomy, Washington State University, Pullman, WA 99163-2814, USA*

<sup>2</sup>*Department of Physics, The Ohio State University, 191 Woodruff Avenue, Columbus, OH 43210, USA*

Accepted . Received ; in original form 2014

## ABSTRACT

This paper explores the integrated-light characteristics of the Milky Way (MW) bulge and to what extent they match those of elliptical galaxies in the local universe. We model composite stellar populations with realistic abundance distribution functions (ADFs), tracking the trends of individual elements as a function of overall heavy element abundance as actually observed in MW bulge stars. The resultant predictions for absorption feature strengths from the MW bulge mimic elliptical galaxies better than solar neighborhood stars do, but the MW bulge does not match elliptical galaxies, either. Comparing bulge versus elliptical galaxies, Fe, Ti, and Mg trend about the same for both but C, Na, and Ca seem irreconcilably different.

Exploring the behavior of abundance compositeness leads to the concepts of “red lean” where a narrower ADF appears more metal rich than a wide one, and “red spread” where the spectral difference between wide and narrow ADFs increases as the ADF peak is moved to more metal-rich values. Tests on the systematics of recovering abundance, abundance pattern, and age from composite stellar populations using single stellar population models were performed. The chemical abundance pattern was recovered adequately, though a few minor systematic effects were uncovered. The prospects of measuring the width of the ADF of an old stellar population were investigated and seem bright using UV to IR photometry.

**Key words:** Galaxy : bulge — galaxies: abundances — galaxies: evolution — galaxies: elliptical and lenticular, cD — galaxies: stellar content

## 1 INTRODUCTION

For the better part of a century, the pursuit of chemical abundances in astronomical objects has driven scientific innovation in the hope of better understanding the origin and evolution of the universe and the objects in it. Recently, this quest has extended to the integrated light of early type galaxies, which seem to have heavy element abundance ratio patterns that both do and do not fit those seen in the Milky Way galaxy (MW), e.g., Johansson et al. (2012).

Stellar abundances for stars in the MW that span a large range of  $[\text{Fe}/\text{H}]$  show a pattern of heavy element enrichment that is largely consistent with two sources for chemical enrichment, Type II and Type Ia supernovae, where the ratio of Type Ia products increases with increasing metallicity<sup>1</sup> (Wheeler et al. 1989). Type II supernovae, the core

collapses and bounces of massive stars, are thought to be rich in elements seeded by  $^{12}\text{C}$  plus the addition of  $^4\text{He}$  nuclei, termed alpha-capture elements, or  $\alpha$  elements for short. They thus include even-numbered elements O, Ne, Mg, Si, S, Ar, Ca, Ti, and possibly Cr, although Cr is more often included in the group of elements termed the iron peak. Type Ia supernova, runaway deflagration obliterations of white dwarfs, have a signature more tilted toward the iron peak group, though some models produce substantial quantities of Si, S, Ar, Ca, and Ti as well (Nomoto et al. 1997). Since the two sources are so disparate in origin, it is not difficult to imagine many ways in which the relative proportions could be made to shift and mix in different ways in different environments. Possible causal variables include the time in-

licity” as  $[\text{M}/\text{H}] \approx \log Z/Z_{\odot}$ , where  $Z$  is the mass fraction of heavy elements. We assume in this work that a stellar evolutionary isochrone at fixed  $Z$  will not vary with detailed chemical mixture, because isochrone sets that do have yet to be computed.

\* E-mail: baitian.tang@email.wsu.edu (BT)

† E-mail: gworthey@wsu.edu (GW)

<sup>1</sup> Contrary to stellar spectroscopy tradition, we define “metal-

terval since star formation, the mass function at formation, the binary fraction, and the heavy element composition.

There is now a plethora of evidence that this two-source picture is too simple (e.g. Edvardsson et al. 1993) especially when stars from dwarf spheroidal satellite galaxies are considered (e.g. Geisler et al. 2005; Shetrone et al. 2001, 2003) and also when MW bulge stars are considered (e.g. Fulbright et al. 2007; Bensby et al. 2013; Meléndez et al. 2008). To explain the discrepancies, it is further hypothesized that the Type II enrichment pattern may change with progenitor mass and progenitor chemical abundance (Fulbright et al. 2007).

More evidence of multiple sources of enrichment is found in the integrated light of early type galaxies. The initial result that more massive elliptical galaxies had higher  $[\text{Mg}/\text{Fe}]$  (Worthey et al. 1992) was satisfactorily explained as a Type II/Type Ia ratio effect. But Worthey (1998) considered more elements (Na, Ca, and N) and could not reconcile the trends in MW disk, MW bulge, and elliptical galaxies under a two-source model.

The MW bulge has the potential to be a good analog for elliptical galaxies, being a spheroidal component of the Galaxy and having a stellar age that predates most of the disk (Ortolani et al. 1995; Zoccali et al. 2003), and yet being near enough so that individual stars can be studied in some detail. In that spirit, Terndrup et al. (1990) made integrated light models by integrating the observed bulge luminosity function of the giants, predicting TiO strengths and  $VJHK$  colors. Both bulge stars and local stars were used as spectral templates. The fascinating conclusion of comparisons of those models with elliptical galaxies is that the bulge template matched better than the solar neighborhood template.

Using this conclusion as a springboard, we explore in this paper firstly the idea that using bulge templates is a superior match to early type galaxies using additional observables than Terndrup et al. (1990) and secondly the hypothesis that elemental ratio changes are the cause.

To our goals adequately, the issue of compositeness in the stellar populations must be addressed. Compositeness is a term that in general would encompass mixtures of stellar population ages and abundances. However, in cases of systems that formed most of their stars in the first half of the universe's existence, the issue of age is strongly suppressed due to (1) the strong decline of stellar population luminosity with increasing age (Bruzual & Charlot 1993) combined with (2) the approximate three-halves rule (Worthey 1994) that states that, for example, a factor of three youthening of a population can be counterbalanced by a factor of two increase in metallicity and the integrated spectrum will change very little. By virtue of the fact that a factor of three in age looms large against the age of the universe for an old population, but a factor of two is small in comparison to the range of two to three orders of magnitude for overall heavy element abundance, it follows that compositeness in age is very minor in effect compared to compositeness in heavy element abundance.

This paper is organized as follows: Composite stellar populations (CSPs) with metallicity-dependent chemical composition are illustrated in § 2. After that, we confront the models with observables from three elliptical samples in

§ 3. The implications are discussed in § 4, and then a brief summary of the results is given in § 5.

## 2 COMPOSITE STELLAR POPULATIONS WITH METALLICITY-DEPENDENT CHEMICAL COMPOSITION

An aspect of compositeness that might conceivably have been present in Terndrup et al. (1990) is that stars of inappropriate heavy element abundance may have been inserted into the luminosity function model.

**Models:** A version of integrated-light models (Worthey 1994; Trager et al. 1998) that use a new grid of synthetic spectra in the optical (Lee et al. 2009) in order to investigate the effects of changing the detailed elemental composition on an integrated spectrum was used to create synthetic spectra at a variety of ages and metallicities for single-burst stellar populations.

For this work, we adopt the isochrones of Bertelli et al. (2008, 2009) using the thermally-pulsing asymptotic giant branch (TP-AGB) treatment described in Marigo et al. (2008). This treatment is calibrated by comparing with AGB stars in the Magellanic Clouds. Perhaps due to counting statistics (Frogel et al. 1990; Santos & Frogel 1997; Bruzual & Charlot 2003; Salaris et al. 2014), the numbers of AGB stars might be over-predicted (Girardi et al. 2010; Girardi et al. 2013) in this model version. Indeed, Tang & Worthey (2013) found abruptly reddened  $V - K$  for metal poor SSPs at the age of 0.1, 1 and 2 Gyr from this isochrone set. For now, however, our main concern is the optical wavelength region, so we are insulated from this effect. Furthermore, the models are modular as regards isochrone libraries, and swapping from one set to another does not affect our conclusions.

Following Poole et al. (2010), stellar index fitting functions were generated from indices measured from the stellar spectral libraries of Valdes et al. (2004) and Worthey et al. (2014b), both transformed to a common  $200 \text{ km s}^{-1}$  spectral resolution. Multivariate polynomial fitting was done in five overlapping temperature swaths as a function of  $\theta_{eff} = 5040/T_{eff}$ ,  $\log g$ , and  $[\text{Fe}/\text{H}]$ . The fits were combined into a lookup table for final use. As in Worthey (1994), an index was looked up for each bin in the isochrone and decomposed into “index” and “continuum” fluxes, which added, then reformed into an index representing the final, integrated value after the summation. This gives us empirical index values. After that, additive index deltas were applied as computed from the grid of Lee et al. (2009) synthetic spectra when variations in chemical composition are needed. The grid of synthetic spectra is complete enough to predict nearly arbitrary composition changes.

**Abundance errors:** Regarding error propagation from individual stars to integrated light, the calibration of the indices depends directly upon high resolution analysis in that the hundreds of local stars that are fit have stellar atmospheric parameters and abundances taken from the body of previous high resolution work. We therefore expect systematic drift (from that source) approximately equal to the error in the mean. For argument's sake, if the scatter is 0.2 dex, and the sample is 100 stars, the systematic drift should be of order  $\sigma_{sys} \approx 0.2/\sqrt{100} = 0.02$ . True errors from this

source will be smaller for well populated parts of the HR diagram such as G dwarfs and K giants.

Mildly more serious is a systematic effect from the Milky Way itself in that the local stellar  $[X/Fe]^2$  trends are frozen into the index fits. If these are not scaled-solar then they introduce systematic drifts. Examining results from local stars, however, and concentrating on thin disk stars only, e.g. (Chen et al. 2000; Bensby et al. 2003, 2014; Reddy et al. 2006), the  $[X/Fe]$  trends versus  $[Fe/H]$  appear flat within a 0.1 dex range for stars near solar metallicity ( $[O/Fe]$  might have a stronger tilt than that, but it is difficult to tell within the increased uncertainty of this element), and scatterlings appear in substantial numbers if thick disk stars are included. A unified high resolution study of the exact sample of stars that enter the low-resolution index fits has not been done. We therefore must presume that the stars fitted obey the average trend. In integrated light, fortunately, these stars are weak-lined and few in number, leading to a few-hundredths change in overall  $[X/Fe]$  for unfavorable cases. Overall, we expect that systematic abundance errors are a few hundredths of a dex for most  $[X/Fe]$ , but higher for elements that are difficult to measure with high resolution spectroscopy (C, N, and O, for example) (Grevesse et al. 2007; Asplund et al. 2009; Ryde et al. 2010).

The most serious systematic error is a purely integrated-light problem arising from modeling uncertainties in stellar temperatures along the isochrone. Temperature changes masquerade as either age or  $[M/H]$  drifts, rendering an absolute  $[M/H]$  quite uncertain. This does not, however, affect  $[X/Fe]$  measurements except via subtle amplification/attenuation effects if the  $[M/H]$  is chosen incorrectly.

**Other caveats:** Observed indices that the model grids simply do not cover occur from time to time. Reasons are as follows. The observational errors (in this work) are not dominated by photon statistics or wavelength solution errors. Errors in matching line of sight velocity dispersion are present, and might contribute more strongly. But the dominant error in the observations is probably relative fluxing, in the sense of incomplete removal of instrumental signatures in the spectrophotometric shape over tens or hundreds of angstroms of wavelength span. Evidence that this effect is serious can be found in that indices with larger wavelength spans in their definitions from blue side to red side often drift more from the models than narrower ones. Also, this defect shows up more in weaker features than in stronger ones.

On the model side, the index fitting functions rest upon stellar spectra for which the fluxing is imperfect as well, and so the same kinds of fluxing effects can be expected at a modest level from the stellar index fitting process as well. The fitting process also runs the risk of oversimplifying the behavior of the indices with stellar parameters.

## 2.1 Abundance Distribution Functions (ADFs)

In the process of making composite stellar populations with single-burst ages but composite abundance distribution functions (ADFs) there is clear empirical guidance for

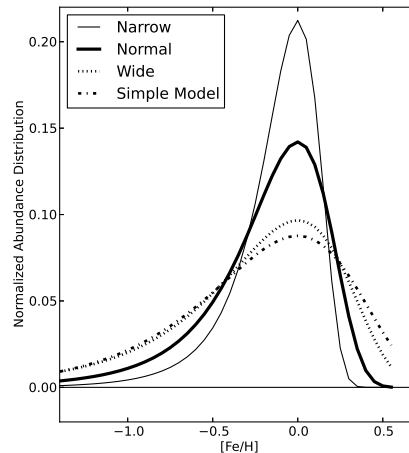


**Figure 1.** The four analytical ADFs we consider are shown, normalized to integral unity given bin widths of 0.1 dex, and set to peak at solar abundance. The ADFs come in narrow (thin line), normal (thick line), and wide (dotted line) variants of the rational decreasing yield model, and the still-wider one zone Simple Model with yield = 0 (dash-dot line). The most metal rich population we can consider is  $[M/H] = 0.65$  due to model limitations.

the shape of the function. It has been clear for many years that the simplest one-zone, constant-yield, no inflow, no outflow, instantaneous-recycling model of chemical evolution produces too many metal-poor stars compared to observations in the solar neighborhood (e.g. Pagel 1997). It has also become clear in recent years that other chemically-evolved places in the universe also have ADFs that are more narrow than the Simple model (Worthey et al. 1996, 2005).

Figure 1 shows the Simple Model for the case of heavy element yield equal to the solar value, along with the analytical function variants that we adopt in this study. A convenient analytical function is the rational decreasing yield formula from Worthey et al. (2005). It narrows the Simple model by having the yield start high and decrease with increasing metallicity. We use parameters  $p = 0.00019$  and  $\epsilon = 0.004$  in the formula for a smooth curve that has a FWHM of 0.62 dex, and we call it our normal width ADF. From there, we scale the width a factor of 1.5 narrower (narrow-width ADF), or a factor of 1.5 wider (wide-width ADF), and also transform it along the  $[M/H]$  axis, as desired. The Simple Model is the widest of all, at a FWHM of 1.06 dex.

While the rational decreasing yield model is not a complete physical model in itself, it does a good job of reproducing the observations, some of which are summarized in Figures 2 and 3. Note that some authors, e.g., Hill et al. (2011); Babusiaux et al. (2010); Ness et al. (2013), argue that the MW bulge ADF is a multiple-peaked function that plausibly represents distinct stellar populations. Without contradicting that in the slightest, we pragmatically note that the match between the observed and model ADFs is nevertheless fairly good, especially in an integrated sense, and so we use the single-peaked function throughout this paper.

<sup>2</sup> “X” represents any one of the heavy elements discussed in this work.

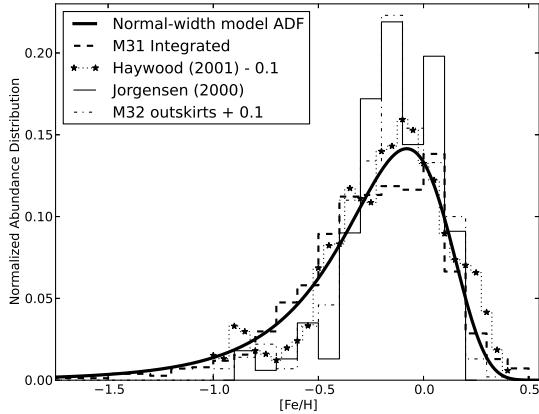


**Figure 2.** Observed ADFs are compared, normalized to integral one with a bin width of 0.1 dex along the  $[\text{Fe}/\text{H}]$  axis. Also shown is our normal width fitting function (heavy line), set to peak at  $[\text{Fe}/\text{H}] = -0.1$ . Other observed cases are M31, considered as a whole (dashed histogram) from photometry of red giants (Worthey et al. 2005)), a field with mostly M32 stars (dash-dot histogram) also from photometry (Worthey et al. 2004) and shifted to the right by 0.1 dex for comparison, and two solar cylinder analyses, one from Jørgensen (2000) (thin solid histogram) and one from Haywood (2001), with corrections to the whole cylinder taken from Wyse & Gilmore (1995) and shifted 0.1 dex to the left for comparison. Roughly, the observed ADFs are comparable in width to, or a bit narrower than, the analytical function.

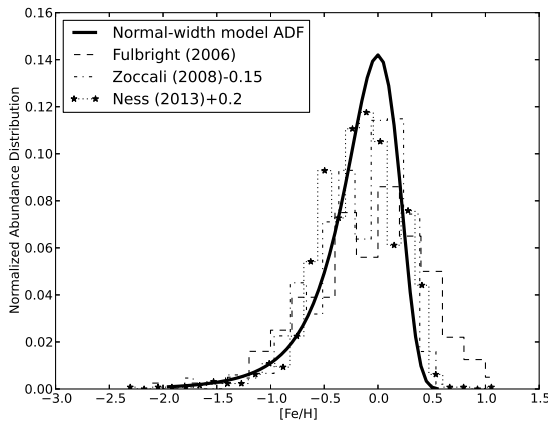


**Figure 3.** Milky Way Bulge ADFs from Fulbright et al. (2006); Zoccali et al. (2008); Ness et al. (2013) (dashed, dash-dotted, and star-marked dotted lines, respectively) are shown in comparison with the normal-width analytical function (bold line).

## 2.2 Milky Way Bulge Chemical Composition

Our composite models are sensitive to element ratios, and the trends of element ratios are included as a function of  $[\text{M}/\text{H}]$ . For incorporation into the models,  $[\text{Fe}/\text{H}]$  and  $[\text{X}/\text{Fe}]$  are treated with exactitude at the spectral library level, but at the isochrone level  $[\text{Fe}/\text{H}]$  is equated with  $[\text{M}/\text{H}]$  due to the lack of elemental mixture sensitivity in the isochrones.

The MW bulge literature abundance measurements come from the following sources.

(i) Meléndez et al. (2008) acquired high resolution near infrared spectra of 19 MW bulge giants. C, N, O and Fe abundances were obtained by spectrum synthesis of a number of lines from the MARCS (Gustafsson et al. 2008) 1D hydrostatic model atmospheres.

(ii) Using similar methods as Meléndez et al. (2008), Ryde et al. (2010) showed the C, N, and Fe abundances of 11 MW bulge giants. We exclude one outlier: Arp 4203, due to its unusual C and N abundances.

(iii) Alves-Brito et al. (2010) observed optical spectra of 25 Galactic bulge giants in Baade’s window. O, Na, Mg, Al, Si, Ca, Ti and Fe abundances were derived from 1D local thermodynamics equilibrium analysis using Kurucz (Castelli et al. 1997) and MARCS models. We choose the abundance ratios determined by MARCS models for consistency among different sets of measurements. These author’s oxygen abundances are excluded, because oxygen’s trend is much different than the other samples at super-solar metallicity. In addition, Alves-Brito et al. argue that the oxygen abundances obtained from several IR OH lines (e.g., Meléndez sample) are preferable to these determined from only one or two optical forbidden lines.

(iv) Bensby et al. (2013) presented element abundance analysis of 58 dwarf and sub-giant stars in the MW bulge using microlensed spectra. MARCS model stellar atmospheres with Fe I NLTE (non-local thermodynamic equilibrium) corrections were employed to extract the stellar parameters.

(v) Hill et al. (2011) performed observations upon a sample of stars in the Baade’s window with GIRAFFE spectrograph at the VLT. Mg and Fe abundances were derived in 163 bulge clump giants using the MARCS models.

(vi) Johnson et al. (2012) presented Na, Al, and Fe abundances of 39 red giant branch (RGB) stars and 23 potential inner disk red clump stars located in Plaut’s window, while Johnson et al. (2013) showed the abundances of  $[\text{Fe}/\text{H}]$ ,  $[\text{O}/\text{Fe}]$ ,  $[\text{Si}/\text{Fe}]$ , and  $[\text{Ca}/\text{Fe}]$  for 264 RGB stars in three Galactic bulge off-axis fields. Note that these abundances are calculated relative to Arcturus. In order to consist with other sources which use solar abundances as reference, we adjust the reported abundances by adding the Arcturus abundances reported by Johnson et al.

(vii) Rich et al. (2005, 2007, 2012) collected a total of 61 bulge giants using NIRSPEC at the Keck telescope. They derived abundances for Fe, C, O and four  $\alpha$  elements (Mg, Si, Ca, and Ti) with reference solar abundances from Grevesse & Sauval (1998).

To incorporate the empirical abundance trends into our integrated-light models, we fit the observed  $[\text{X}/\text{Fe}]-[\text{Fe}/\text{H}]$  relations. We use a one-error least square fitting, in which the variances of  $[\text{X}/\text{Fe}]$  are considered as weights during the procedure of finding the minimum  $\chi^2$ . We adopt an uncertainty of 0.10 dex for the Meléndez sample and 0.11 dex, 0.09 dex for C and N abundances in the Ryde sample. Most of the abundances in the other data sets have individual errors, and the few without error estimates are excluded before the fitting. For simplicity, we consider only two possible fitting functions, a linear function or a quadratic function. The better one is chosen after individual inspection for both.

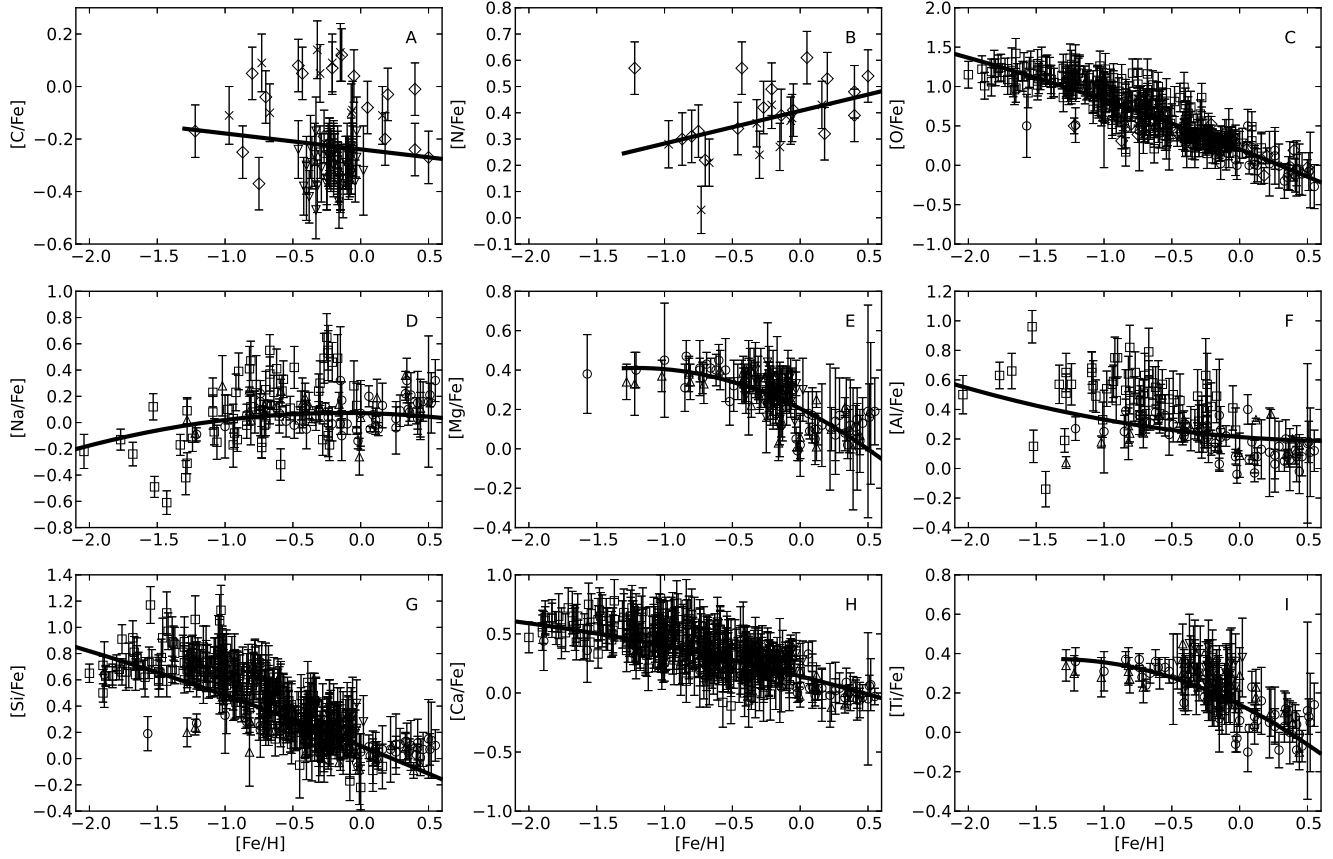


**Figure 4.** Abundance trends in the Milky Way bulge. Measurements from Rich et al. (2005, 2007, 2012) (open downward triangles), Johnson et al. (2012, 2013) (open squares), Hill et al. (2011) (open pentagons), Bensby et al. (2013) (open circles), Alves-Brito et al. (2010) (open upward triangles), Ryde et al. (2010) (crosses) and Meléndez et al. (2008) (open diamonds) are shown. Our fits are shown as thick solid lines. Errorbars are the published uncertainties.

- C and N

Most of the carbon abundances from Meléndez et al. (2008); Ryde et al. (2010) are close to solar, while Rich et al. derived sub-solar abundances  $[C/Fe] \sim -0.2$ . This disparity might originate from the complexity of infrared spectral feature lines: C, O, and other stellar parameters are obtained by simultaneous spectral fitting of several CO and OH molecular bands, which are sensitive to temperature, gravity and micro-turbulence (Origlia et al. 2002). In the cases of C and N, one might be concerned with alterations in surface abundance due to dredge up of nucleosynthetic processes. In the case of carbon, the mere fact that carbon abundances are near-solar or even sub-solar imply that the third dredge-up has not brought up significant amount of CNO-cycled rest-products to the surface (Meléndez et al. 2008). However, super-solar nitrogen abundances are observed and seem to require extra sources besides the CNO cycle such as the neutrino process in massive stars suggested by Timmes et al. (1995) or primary nitrogen. In this work, we model  $[C/Fe]$  and  $[N/Fe]$  as linear functions of  $[Fe/H]$  (Figure 4A and 4B).

- O and Mg

According to the abundance yields of type II supernovae (e.g.: Woosley & Weaver 1995), O and Mg are two of the primary alpha elements produced, and they are produced in almost the same ratio for stars of disparate mass and progenitor heavy element abundance. In Figure 4C and 4E, O differs from Mg below  $[Fe/H] \sim -1$ , due to the scarcity of available data points for  $[Mg/Fe]$  at these metallicities. We fit them with quadratic functions.

- Na and Al

Na and Al are closely affected by the excess neutrons associated with  $^{22}\text{Ne}$  generation (the beta decay of  $^{18}\text{F}$  to  $^{18}\text{O}$ ) during the helium burning (Arnett 1971; Clayton 2007). In Figures 4D and 4F,  $[Na/Fe]$  is an increasing function of  $[Fe/H]$ , while  $[Al/Fe]$  decreases as metallicity increases. We fit them with quadratic functions.

- Si, Ca, and Ti

Based on the similar trend of Si, Ca, and Ti as a function of  $[Fe/H]$ , we fit these three elements with quadratic functions (Figures 4G, 4H, and 4I). These three elements are grouped together as explosive alpha elements sharing a similar nucleosynthetic origin. However, they do not show

the same trend in elliptical galaxies (Worthey et al. 2011, 2014a; Conroy et al. 2014). We search for the physical reason underlying this disorder of facts in § 4.

Generally speaking, the overall trend is clear in all the panels of Figure 4, but the scarcity of data for  $[\text{Fe}/\text{H}] < -1.0$  renders the detailed form of the function vague for some elements. When integrated, the fraction of metal poor stars is small in elliptical galaxies, so the uncertainty of fitting function at  $[\text{Fe}/\text{H}] < -1.0$  does not affect our conclusions.

### 2.3 300 km s<sup>-1</sup> Elliptical Galaxy Chemical Composition

Since elliptical galaxies also seem to have a unique chemical composition but we do not have the luxury of star-by-star chemical analysis, we assume abundance ratios that are constant at all  $[\text{M}/\text{H}]$ . We incorporate the most up-to-date elliptical galaxy abundance ratios into our CSP models, and call that variant the EG CSP. Johansson et al. (2012); Worthey et al. (2014a) and Conroy et al. (2014) have obtained the abundances of several major elements from the integrated light spectra. Given the disparities of their methods, it gives confidence that the final results are generally consistent with each other (See Conroy et al. 2014). In this work, we adopt the set of element abundance ratios extracted from stacked 300 km s<sup>-1</sup> SDSS early-type galaxy spectra, namely,  $[\text{C}/\text{Fe}]=0.21$ ,  $[\text{N}/\text{Fe}]=0.27$ ,  $[\text{O}/\text{Fe}]=0.28$ ,  $[\text{Na}/\text{Fe}]=0.43$ ,  $[\text{Mg}/\text{Fe}]=0.22$ ,  $[\text{Al}/\text{Fe}]=0.0$ ,  $[\text{Si}/\text{Fe}]=0.16$ ,  $[\text{Ca}/\text{Fe}]=0.02$ ,  $[\text{Ti}/\text{Fe}]=0.12$ , set to be constant at all  $[\text{M}/\text{H}]$ .

## 3 RESULTS

In this section, we show several indices for the three CSPs that we assemble: 1. CSPs with scaled solar element abundances (SS CSPs, solid lines); 2. CSPs with Galactic bulge element abundances (GB CSPs, dashed lines); 3. CSPs with 300 km s<sup>-1</sup> elliptical galaxy element abundances (EG CSPs, dotted lines). We compute the CSPs at the age of 2, 4, 6, 8, 10, 12, and 14 Gyr with five shifted  $[\text{M}/\text{H}]$  distributions: peak  $[\text{M}/\text{H}] = -0.4, -0.2, 0.0, 0.2, 0.4$ . We present model indices at  $\sigma = 300$  km s<sup>-1</sup> resolution, where the transformation from 200 km s<sup>-1</sup> to 300 km s<sup>-1</sup> is accomplished via smoothing of synthetic model spectra.

**Observational material:** Three sources are used for galaxy indices in Figure 5, which displays how well a bulge template matches elliptical galaxy observations.

(i) Graves et al. (2007) presented an analysis of red sequence galaxy spectra ( $0.06 < z < 0.08$ ) from the SDSS, which uses a dual-fiber spectrograph, with resolution  $R \approx 1800$ , wavelength coverage  $\lambda = 3800 - 9200\text{\AA}$ , and fiber diameter  $d = 3''$  which translates to physical scales between 3.4 and 4.6 kpc. They labeled the red sequence galaxies with neither  $\text{H}\alpha$  or  $[\text{O II}]$  detected (at the  $2\sigma$  level) as “quiescent” galaxies, and divided these quiescent galaxies ( $N=2000$ ) into 6 bins in velocity dispersion ( $\sigma = 70 - 120, 120 - 145, 145 - 165, 165 - 190, 190 - 220$ , and  $220 - 300$  km s<sup>-1</sup>). All the spectra were broadened to  $\sigma = 300$  km s<sup>-1</sup> before stacking. The indices extracted from the stacked spectra are represented by open diamonds in Figure 5.

(ii) Trager et al. (2008) obtained the spectra of 12 early-type galaxies in the Coma cluster with  $41 < \sigma < 270$  km s<sup>-1</sup>, including the cD galaxy NGC 4874. The slitlet spectra were corrected along the slit to mimic a circular aperture of  $2''.7$ , which corresponds to a physical diameter of 637 pc. These spectra were smoothed to  $\sigma = 300$  km s<sup>-1</sup>. Indices are shown as filled squares in Figure 5.

(iii) Serven (2010) presented spectra of mostly Virgo elliptical galaxies with  $80 < \sigma < 360$  km s<sup>-1</sup>. The observations were taken by the Cassegrain Spectrograph mounted on the 4m Mayall telescope at Kitt Peak National Observatory. Serven extracted the spectra at an aperture of  $13''.8$ , which corresponds to a physical diameter of 1.1 kpc for most of the galaxies (the ones in the Virgo cluster), and then smoothed the spectra to  $\sigma = 300$  km s<sup>-1</sup>. This sample is denoted by blue triangles in Figure 5.

**Age and Metallicity:** Balmer line index – iron index plots are known to partially break the age-metallicity degeneracy that otherwise prevails in most diagrams (Worthey 1994).  $\langle \text{Fe} \rangle^3$  (González 1993) is sensitive mainly to elemental Fe and thus is a good analog of  $[\text{Fe}/\text{H}]$ .  $\text{H}\beta$  is widely used as an age indicator due to its nonlinear response to main-sequence turnoff temperature. Compared to bluer  $\text{H}\delta_F$ ,  $\text{H}\beta$  is more susceptible to nebular emission contamination. We apply nebular emission corrections for  $\text{H}\beta$  and  $\text{H}\delta_F$  to the Graves sample and Serven sample following the recipe of Serven & Worthey (2010). Five emission-corrected galaxies in the Serven sample are labelled as open triangles, since larger uncertainties might be expected for these galaxies in plots involving Balmer features. Figures 5A and 5B show that the inferred ages are consistent with the expectation that elliptical galaxies are generally old and metal rich. One obvious exception is found at the top of Figs. 5A and 5B: NGC 3156, a small elliptical galaxy with clear signs of a recent burst of star formation (Kuntschner et al. 2006).

All age-sensitive diagrams agree that elliptical galaxies are slightly more metal rich than the GB, since we model the GB with a peak metallicity of solar, while the elliptical galaxies in Fig. 5 cluster around the +0.2 peak line.

**Iron:** Figure 5C, the  $\text{Fe}4383 - \langle \text{Fe} \rangle$  plot, is highly degenerate, showing similar effects of target elements on  $\text{Fe}4383$  and  $\langle \text{Fe} \rangle$ ; that is, both indices are sensitive to Fe, age, and overall abundance at approximately the same rate. Compared with SS CSPs, GB CSPs and EG CSPs shift toward weaker values of  $\langle \text{Fe} \rangle$  by about 0.1 Å. This is an artifact of the fact that  $[\text{M}/\text{H}]$  is held constant, so that enhancement of the target elements comes at the expense of Fe (c.f., the analytical derivation in Johansson et al. (2012)). Restricted to Fe-sensitive indices, SS, GB, or EG mixtures are all able to reproduce the observations.

**Carbon and Nitrogen:** In the  $\text{C}24668 - \langle \text{Fe} \rangle$  plot (Fig. 5D), EG CSPs shift upward, but GB CSPs shift downward with respect to SS CSPs. This is because  $\text{C}24668$  is mainly controlled by  $\text{C}_2$  with additional contributions from Fe, Mg, Cr, and Ti (Worthey et al. 1994) plus the evident fact that  $[\text{C}/\text{Fe}] \sim -0.2$  for the GB but  $[\text{C}/\text{Fe}] = 0.21$  for EG. The observations lie close to the EG CSPs, but the GB is apparently not a good template for this spectral region.

Regarding Fig. 5E,  $\text{CN}_1$  is known to closely depend on

<sup>3</sup>  $\langle \text{Fe} \rangle = (\text{Fe}5270 + \text{Fe}5335)/2$ .

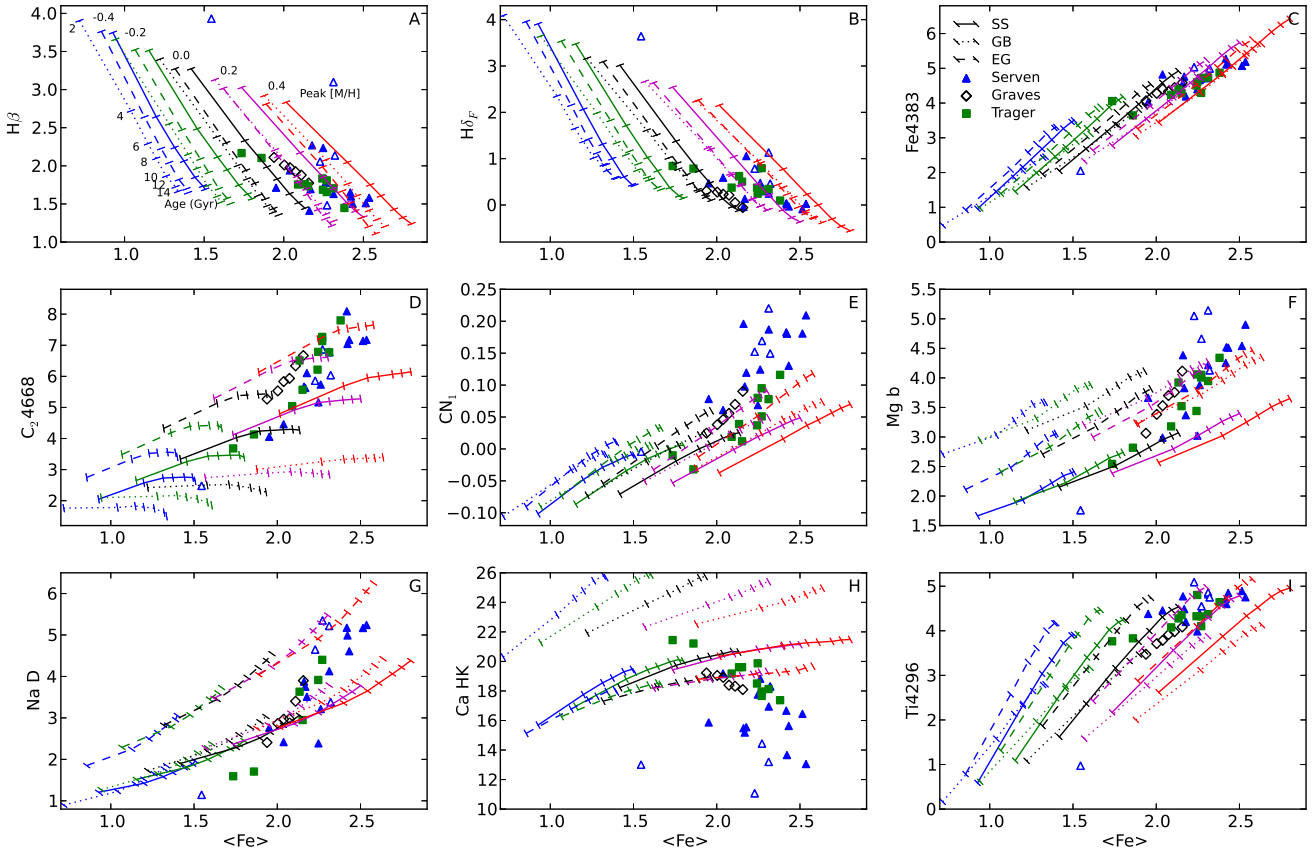


**Figure 5.** Integrated light index diagrams, all versus  $\langle \text{Fe} \rangle$ . CSP models with ADF peaks at  $[\text{M}/\text{H}] = -0.4, -0.2, 0, 0.2, 0.4$  dex (blue, green, black, magenta and red lines, respectively) are shown for three chemical mixtures, SS CSPs (solid lines), GB CSPs (dotted lines), and EG CSPs (dashed lines). Ages (2 through 14 Gyr in steps of 2 Gyr) are shown as ticks along the lines. Serven (blue triangles), Graves (open diamonds), and Trager (green squares) observations are shown. Five Balmer emission galaxies in the Serven sample (open blue triangles) have had additional corrections applied.

C, N, and O (Serven et al. 2005). The fact that GB CSPs and EG CSPs overlap means that the amalgamated effects wrought by C, N, and O are almost the same in these two CSPs, despite the individual abundance ratios being different ( $[\text{C}/\text{Fe}] \sim -0.2$ ,  $[\text{N}/\text{Fe}] \sim 0.3$ ,  $[\text{O}/\text{Fe}] \sim 0.3$  for GB<sup>4</sup>,  $[\text{C}/\text{Fe}] = 0.21$ ,  $[\text{N}/\text{Fe}] = 0.27$ ,  $[\text{O}/\text{Fe}] = 0.28$  for EG). In Fig. 5E, the GB and EG CSPs shift upward, showing somewhat better agreement with the data points than SS CSPs. Some of the data points, especially the Serven sample, are stronger-lined than the model grid. Partly, that is an artifact of taking an average value for the models, but it might also be because the apertures of the Serven spectra concentrate on the nuclei of the galaxies, zeroing in on the most extremely metal rich stellar populations and also magnifying near-nuclear effects such as lingering star formation or low level Active Galactic Nuclei (AGN) activity.

**Magnesium:** Mg, one of the primary alpha elements, is observed to be enhanced in massive elliptical galaxies

(Worthey et al. 1992; Conroy et al. 2014) and its strong absorption feature at  $5170\text{\AA}$  is found to be closely related to galactic velocity dispersion (Burstein et al. 1984; Davies et al. 1993; Bender et al. 1993; Trager et al. 2000; Sánchez-Blázquez et al. 2006a). In Figure 5F, GB CSPs and EG CSPs show a much better match to the data points than SS CSPs. The stellar observations in the bulge and elliptical galaxies imply  $[\text{Mg}/\text{Fe}] \sim 0.21$ , and this appears an adequate match to the data.

**Sodium:** Na D, a strong absorption feature in the optical, has complex contributing factors. Na D is very sensitive to the Na abundance and is somewhat sensitive to the initial mass function (IMF), but it also suffers from possible interstellar absorption (Worthey et al. 1994). In Figure 5G, we find that the locus of GB CSPs is not sufficient to match all the data points. On the other hand, the EG CSP value of  $[\text{Na}/\text{Fe}] = 0.43$  seems to miss the average and match only the most Na-strong elliptical galaxy data points. In our models, the IMF is set to a Salpeter one, and although IMF variation is not the subject of this paper, model experiments show

<sup>4</sup> From § 4.3

that IMF variation causes only minor changes in the Na D index, leading Jeong et al. (2013), for example, to conclude that the Na abundance in Na excess objects might be truly enhanced.

**Calcium:** Ca HK, first defined in Serven et al. (2005), was employed to study the Ca abundance in Worthey et al. (2011) in part due to its insensitivity to the IMF. Given that Ca is one of the alpha elements and Ca yields closely track Mg (Nomoto et al. 2006; Kobayashi et al. 2006), the decreasing trend of Ca HK as a function of elliptical galaxy velocity dispersion is puzzling. Worthey et al. (2011) nevertheless concluded that chemical abundance variation is the explanation for the unusual Ca HK behavior. In Figure 5H we see that enhanced  $[\text{Ca}/\text{Fe}]$ , as in the GB CSPs, drives the model grids even further away from the data points. When we look at the EG CSPs,  $[\text{Ca}/\text{Fe}] = 0.02$ , and we would expect almost no change in Ca HK, but because other element ratios are changing, especially Mg, the model Ca HK index drops lower. However, even the amalgamated effects of all the target elements are insufficient to cover the data points. The problem is eased when one notes that the Serven sample might lie low due to a spectral response systematic (Worthey et al. 2011).

**Titanium:** Ti, the heaviest alpha element, is found to display little evidence of varying as a function of velocity dispersion in elliptical galaxies (Conroy et al. 2014; Worthey et al. 2014a). Here, we estimate Ti abundance by adopting a rarely used Ti index, Ti4296. The Ti4296 –  $\langle\text{Fe}\rangle$  plot looks similar to a inverted Balmer lines –  $\langle\text{Fe}\rangle$  plot due to its red pseudocontinuum passband encroaching on  $\text{H}\gamma$ , and therefore has decent capability of breaking the age–metallicity degeneracy. In addition, it has relatively low response to most of the heavy elements (Serven et al. 2005). Figure 5I shows that a scaled solar or mildly enhanced Ti abundance is sufficient for elliptical galaxies.

## 4 DISCUSSION

The clear basic result is that the  $[\text{M}/\text{H}]$ -dependent elemental mixture in the GB is not a good template for massive elliptical galaxies, although the conclusion of Terndrup et al. (1990) that the GB is a better template than local stars also seems perfectly valid. We now go on to discuss some extensions and implications of this work.

### 4.1 Varying the Widths of the ADFs: Red Lean and Red Spread

The width of the ADF is a parameter with significant importance in our CSP models. To measure this width via observed spectra or models is an attractive goal. Some basic properties of the CSP models are summarized in Table 1, where we sample only ages 2 and 12 Gyr, and use ADFs that peak at the solar value. The widths (FWHM) of narrow, normal, wide ADFs are 0.41, 0.62, and 0.93 dex, respectively. Note that our wide-width ADF is almost the same width as the classical Simple model (FWHM 1.06 dex), but has a sharper cutoff at high metal abundance. The weighted means are calculated in the usual way. For example, to compute the  $B$  flux weighted mean metallicity we convert to a pseudoflux and weight as:

**Table 1.** Mean  $[\text{M}/\text{H}]$  for Composite Populations Peaking at  $[\text{M}/\text{H}] = 0$

| Model          | Mass-Weighted<br>[M/H] | $B$ -Weighted<br>[M/H] | $K$ -Weighted<br>[M/H] |
|----------------|------------------------|------------------------|------------------------|
| Narrow, Age 2  | −0.13                  | −0.18                  | −0.15                  |
| Narrow, Age 12 | −0.13                  | −0.20                  | −0.13                  |
| Normal, Age 2  | −0.19                  | −0.29                  | −0.21                  |
| Normal, Age 12 | −0.19                  | −0.31                  | −0.18                  |
| Wide, Age 2    | −0.26                  | −0.42                  | −0.28                  |
| Wide, Age 12   | −0.26                  | −0.46                  | −0.25                  |
| Simple, Age 2  | −0.25                  | −0.42                  | −0.28                  |
| Simple, Age 12 | −0.25                  | −0.46                  | −0.23                  |

$$\overline{[\text{M}/\text{H}]} = \frac{\sum [\text{M}/\text{H}]_i w_i}{\sum w_i}$$

where  $i$  is the index over bins in the ADF,  $w_i = S_i 10^{-0.4B_i}$ ,  $S_i$  is the ADF itself, i.e., the mass fraction of each stellar population, and  $B_i$  is the absolute magnitude of the stellar population at fixed initial mass.

Examination of Table 1 tells us that the mean metallicity is less than the peak metallicity due to the asymmetry of the ADF. Also, the  $B$  band light samples the ADF at about 0.2 dex lower metallicity than the mass-weighted or  $K$ -band-weighted would. This is due to the fact that metal-poor populations are brighter, coupled with the fact that they are also bluer. On the other hand,  $K$  band light balances the effect of brighter (even at  $K$  band) metal poor populations with the color change that boosts the  $K$  output of metal-rich populations so that the net effect at  $K$  is almost the same as the true, mass-weighted mean.

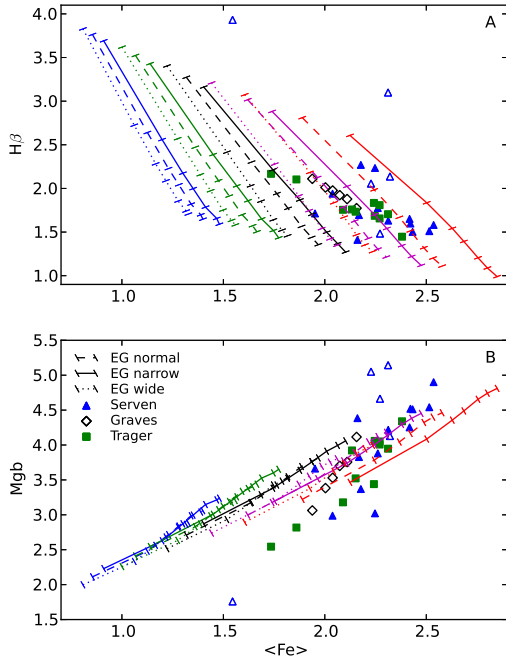
Note that the CSPs investigated in § 3 are modelled with the normal-width ADF.

Figure 6 quantifies the influence of ADF width. Using the EG chemical mixture, we plot narrow width (solid), normal (dashed), and wide (dotted) lines in the  $\text{H}\beta$  –  $\langle\text{Fe}\rangle$  and  $\text{Mgb}$  –  $\langle\text{Fe}\rangle$  plots. The three elliptical galaxy samples from § 3 are plotted along with the CSP model grids.

We see two main effects. The first effect is that the narrower the ADF, the more metal-rich it appears (“red lean”). The second effect is an amplification of the disparity between narrow and wide ADFs as the peak metallicity shifts to higher  $[\text{M}/\text{H}]$  (“red spread”).

Both red lean and red spread originate from the fact that metal poor populations are more luminous than their metal rich counterparts (for the same initial mass). As the width decreases, the more-potent metal-poor fraction decreases, and the overall average moves toward the metal-rich in a light-weighted sense as seen in Table 1, or, in looser words, it leans toward the red. The red spread effect relies upon, in addition, the increased volatility of red giant branch temperatures for cooler, more metal rich stellar populations (cf. Fig 4 of Worthey (1994)) coupled with the backwarming of cooler stars due to increased line-blanketing (Mihalas 1970). The increased  $\Delta T$  and color change from backwarming combine to create a greater spectral change in the metal rich regime than the metal poor regime for the same  $\Delta[\text{M}/\text{H}]$ , and thus an amplified spectral change for the more metal-rich ADFs.





**Figure 6.**  $H\beta - \langle \text{Fe} \rangle$  and  $\text{Mgb} - \langle \text{Fe} \rangle$  plot for narrow (solid lines), normal (dashed lines), and wide (dotted lines) ADFs. Peak  $[\text{M}/\text{H}] = -0.4, -0.2, 0, 0.2, 0.4$  dex are indicated by blue, green, black, magenta and red lines, respectively. We choose EG CSPs for illustration purpose, but other CSPs would not change our conclusions. Elliptical galaxies are labelled the same as Figure 5.

Not all the ADF widths are physically reasonable. With logic similar to that surrounding Figure 2 of Worthey et al. (1996) concerning the Simple Model, the wide-width ADFs seem ruled out by inspection of Figure 6. That is, in order to make a wide-width model match the observed spectral indices of elliptical galaxies, the maximum  $[\text{M}/\text{H}]$  required becomes unreasonably large: Since the peak  $= +0.4$  model still falls short of observation, a wide-width model that matches would have *most* of its stars at  $[\text{M}/\text{H}]$  greater than several times the solar abundance. Although the normal-width ADF (and not the narrow width) fit nicely, we cannot (yet) show evidence from integrated light that would exclude the narrow width ADF, even though star-by-star analyses always show ADFs wider than our narrow model.

## 4.2 Comparing Chemical Compositions of the Milky Way Bulge and Elliptical Galaxies

Throughout this paper, we investigate the possibility of using Milky Way bulge abundance trends to interpret elliptical galaxy observables. What we found in § 3 can be summarized as this: Fe, Mg, and Ti match the elliptical galaxy abundances, but more C, Na and less Ca are required to explain the absorption indices of elliptical galaxies. In other words, MW bulge mimic the elliptical galaxies better than scaled solar stars do, but concrete disparities still exist between the bulge and elliptical galaxies.

The MW bulge and elliptical galaxies both consist of old

stellar populations, but they are otherwise dissimilar. The obvious difference is that the MW bulge is a subcomponent of a spiral galaxy. Also, Tremaine et al. (2002) found MW bulge velocity dispersion is close to  $95 \text{ km s}^{-1}$ , while the mean velocity dispersion of our elliptical galaxies is about  $200 \text{ km s}^{-1}$ . The various nucleosynthetic processes associated with different mass stars are likely the key to understand the element abundance trends in both environments, but we still lack a clear connection between galaxy mass or formation history and nucleosynthetic outcome.

We find more C in elliptical galaxies than in the MW bulge using  $\text{C}_{24668}$ . The N and O abundance can be estimated by including other element-sensitive indices, like  $\text{CN}_1$  and  $\text{TiO}_2$  (Graves et al. 2007; Johansson et al. 2012; Conroy et al. 2014), but since such precise abundance calculation is beyond the scope of this work, we defer the discussion of N and O abundances to other papers such as Worthey et al. (2014a). In terms of C enhancement, many studies show that intermediate mass stars contribute significant amounts of C due to dredge up in the asymptotic giant branch phase (Van den Hoek & Groenewegen 1997; Woosley et al. 2002). But Pipino & Matteucci (2004) found the C abundance generated by these models is lower than the observed values. Recently, Geneva group (Ekström et al. 2012; Georgy et al. 2013) showed rotation in massive stars significantly changes the C yield. In that spirit, Pipino et al. (2009) included stellar rotation in their chemical evolution models and found an increased C abundance which produce a trend consistent with Graves et al. (2007). It is possible that the discrepancy of C abundance between the MW bulge and elliptical galaxies might be also caused by stellar rotation. Following this logic, then for more C we would require more massive stars to form during the evolution of elliptical galaxies, since rotation is more significant for massive stars (Ekström et al. 2012; Georgy et al. 2013). This could mean a top-heavy IMF, but not necessarily because increased effectiveness of massive star yields can be achieved by a Salpeter IMF with a galaxy mass-dependent star formation rate (Pipino et al. 2009).

The case of calcium is even more puzzling. Given the similarity of old stellar populations in the MW bulge and elliptical galaxies, the dichotomous behavior of Ca challenge most of the nucleosynthesis theories. To summarize the empirical evidence: 1. Ca has sub-solar abundance in elliptical galaxies. That Ca feature strengths generally decline with elliptical galaxy velocity dispersion (Saglia et al. 2002) is not a low mass stellar IMF effect (Worthey et al. 2011) but instead a real decline in  $[\text{Ca}/\text{Mg}]$ , a modest decline in  $[\text{Ca}/\text{Fe}]$ , and possibly a small decline in  $[\text{Ca}/\text{H}]$  as well. Near solar or sub-solar Ca abundances are also found by Graves et al. (2007); Johansson et al. (2012); Worthey et al. (2014a). 2. Ca loosely resembles Mg and O in the MW bulge (§ 2 & Fulbright et al. 2007), which seems agree with its alpha element origin, nevertheless Ca in elliptical galaxies approximately follows  $[\text{Fe}/\text{H}]$  (Graves et al. 2007; Johansson et al. 2012; Worthey et al. 2014a; Conroy et al. 2014). According to the Type II supernova yields of Nomoto et al. (2006), Ca and Mg seem in lockstep with each other, trending the same with progenitor mass and metallicity, and leaving a clear impression that Ca should follow Mg always. So what is the reason for this Ca-Mg dissimilarity of the elliptical galaxies? Two scenarios have been proposed to explain Ca's

atypical alpha element behavior under the classic one zone, two sources (Type Ia and II supernova) hypothesis.

(i) Pipino & Matteucci (2004); Pipino et al. (2009) suggested the Ca underabundance relative to Mg found in their chemical evolution models is caused by a non-negligible Ca contribution via Type Ia supernova (Nomoto et al. 1997). According to the delayed detonation model described in Nomoto et al. (1997), Ca yield does come out higher than Mg yield for Type Ia supernova. Following this logic, the enhanced Mg abundance in massive elliptical galaxies would still come from increased Type II contributions, but Ca would be diluted as more Type II products are added. Note that is necessary for Type II supernovae to produce less Ca than current yields predict for this scheme to be successful.

More speculatively, there might be a connection with the recent studies of silicon group elements: Based on the classical W7 models (Nomoto et al. 1984; Thielemann et al. 1986), De et al. (2014) propose the “W7-like” models that is now capable of varying the  $^{22}\text{Ne}$  mass fraction freely. They notice the electron fraction of the progenitor white dwarfs, which anti-correlates with the  $^{22}\text{Ne}$  mass fraction, systematically influences the nucleosynthesis of the silicon group elements (Si, S, and Ca) in the sense that Ca shows a nearly quadratic increasing trend with electron fraction, while Si is almost insensitive to the electron fraction. Observationally speaking, Si is a fair alpha element compared to Ca, since it roughly follows Mg and O in both the MW bulge and elliptical galaxies<sup>5</sup>. Therefore, the observations imply more Ca, but the same amount of Si are generated in low mass ellipticals via Type Ia supernova. The Ca and Si yields would reconcile with the theory of De et al. (2014) if the electron fraction is a decreasing function of stellar velocity dispersion. However, we also notice the dynamical range of electron fraction is small in De et al. (2014), which means an observational demonstration is unlikely.

If the MW bulge is an analog of a low- $\sigma$  elliptical galaxy (MacArthur et al. 2009), its Ca contribution from Type Ia supernova should be higher than massive elliptical galaxies (c.f. Thomas et al. 2011 for a similar statement). Given that the decreasing trend of  $[\alpha/\text{Fe}]$  versus  $[\text{Fe}/\text{H}]$  is usually explained by a Type Ia supernova contribution of Fe (Wheeler et al. 1989), an increase of Type Ia supernova Ca would flatten its negative slope against  $[\text{Fe}/\text{H}]$ , and make Ca dissimilar to other alpha elements. Unfortunately for the Type Ia Ca origin hypothesis, the  $[\text{Ca}/\text{Fe}]$  and  $[\text{Mg}/\text{Fe}]$  trends in Figure 4 look very similar.

(ii) Alternatively, the Ca behavior could be conceived to be the result of Ca yield suppression in massive ellipticals. This conjecture might be caused by a mass-dependent Ca yield in supernova, where the highest-mass stars contribute less Ca but continue to contribute Si, O, and Mg, and massive ellipticals would favor these highest-mass stars. This was suggested long ago (Worthey et al. 1992) but the specific question of Ca yield is ambiguous (Woosley & Weaver 1995; Nomoto et al. 2006). On the other hand, Ca yield suppression might connect with a metallicity-dependent yield. Fulbright et al. (2007) suggested inclusion of metallicity-dependent wind may change the alpha element yields from massive Type II progenitors in Woosley & Weaver (1995).

**Table 2.** Recovery of Population Parameters Under an SSP Hypothesis

| Quantity | Mass-Weighted Value | Recovered Value | Standard Deviation |
|----------|---------------------|-----------------|--------------------|
| Age      | 8                   | 5.7             | 0.9                |
| Age      | 12                  | 10.6            | 2.2                |
| [M/H]    | −0.19               | −0.19           | 0.15               |
| [C/Fe]   | −0.23               | −0.27           | 0.05               |
| [N/Fe]   | 0.38                | 0.14            | 0.09               |
| [O/Fe]   | 0.32                | 0.24            | 0.19               |
| [Na/Fe]  | 0.06                | 0.17            | 0.17               |
| [Mg/Fe]  | 0.25                | 0.25            | 0.14               |
| [Si/Fe]  | 0.17                | 0.25            | 0.03               |
| [Ca/Fe]  | 0.19                | 0.20            | 0.07               |
| [Ti/Fe]  | 0.18                | 0.37            | 0.18               |

As metallicity increases, the yield of hydrostatic elements (e.g., O, Mg) increases and the yield of explosive elements (e.g., Si, Ca, Ti) declines. This seems qualitatively correct. A metallicity-dependent yield has not been systematically studied by any theoretical group to the best of our knowledge.

### 4.3 Recovering Abundances with Simple Stellar Population Models

Efforts to discover the detailed chemical composition of galaxies and most efforts to discover the ages of old stellar populations use single-burst, single-composition simple stellar population (SSP) models. Going from inherently CSP populations but interpreting them via SSP models might introduce systematics. To explore this, we perform the following theoretical exercise.

In Worthey et al. (2014a), a chemical mix-sensitive inversion program that uses SSP based on Bertelli et al. (1994) evolution was applied to several samples of galaxies. Here, we use the same inversion program on the CSP models, built with evolution based upon Marigo et al. (2008) as well as being composite in metallicity. Uncertainties in each index were calculated by a photon noise model normalized to  $S/N = 25$  per Å at 5000Å in  $F_\lambda$  units. The comparison is presented in Table 2 for the average of two ages (8 and 12 Gyr) computed from a CSP model with normal-width ADF peaked at solar abundance and with a run of bulge chemical mixtures and more recent stellar evolution, interpreted with older models under a single-burst hypothesis. As in Worthey et al. (2014a), sensitivities to different elements were turned on and off in order to generate a crude “permutational” estimate of uncertainty.

Table 2 shows approximate agreement between CSP input and SSP-recovered parameters, with interesting systematic drifts. The mean ages drift slightly younger, especially with  $[\text{Si}/\text{Fe}]$  set to zero. Letting  $[\text{Si}/\text{Fe}]$  vary allows the ages to relax about 1.5 Gyr older. This is due to the molecular SiH features in the blue covarying with some of the Balmer indices, from which the bulk of the age information comes. With some permutations of which elements were allowed to vary, there arises a correlation between age and a few of the  $[\text{X}/\text{Fe}]$ , often  $[\text{Na}/\text{Fe}]$  for example. This is slippage in

<sup>5</sup> S is left out due to a lack of spectral lines (Serven et al. 2005).

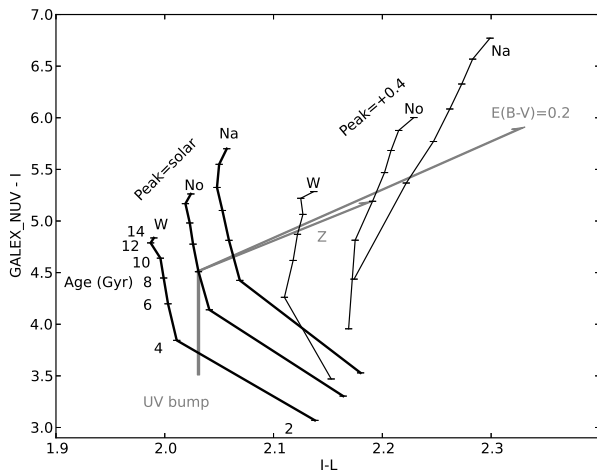


**Figure 7.** Integrated light color-color diagram that shows sensitivity to the width of the ADF involving the GALEX NUV filter ( $0.2 \mu\text{m}$ ) and Johnson-Cousins  $I$  ( $0.7 \mu\text{m}$ ) and  $L$  ( $3.4 \mu\text{m}$ ). Colors are set to zero magnitude for the spectral shape of Vega. As in previous figures, stellar population ages between 2 and 14 Gyr are shown, for three ADF widths (marked “W” for wide, “No” for normal, and “Na” for narrow) and two peak metallicities, peak  $[M/H] = \text{solar}$  (bold lines) and peak  $[M/H] = +0.4$  (thinner lines). The effect of dust screen extinction, the increase of metallicity, and including a hot UV-bump component are illustrated with labelled vectors.

the inversion scheme and a caution for future work with this inversion program. The mean  $[M/H]$  is recovered well. The abundance parameters are adequately recovered, with  $[N/Fe]$  too low, and  $[Ti, Si/Fe]$  too high at marginal statistical significance. Table 2 is encouraging in terms of basic coherence between models and in the fact that the element ratios can be recovered in a way that resembles the actual, metallicity-and-mass-weighted mean. One can also safely say that more work is needed to truly understand all possible systematics.

#### 4.4 Detectability of ADF Width

We are able to fuzzily reject a too-wide abundance distribution, but we are so far unable to distinguish narrow from normal ADFs in integrated light. We now attempt to point a way forward by considering the spectral shape of the composite population as a whole. Compositeness of stellar populations, be it age-composite or abundance-composite, can be expected to increase the variety of stellar temperatures present in the population, and thus increase the width of the overall integrated sum of near-blackbody stellar fluxes. Thus, sampling the spectrum over a broad span of wavelength may yield diagnostic information. We attempt to illustrate how this might work in Figure 7.

We note several encouraging things. In that color plane, age and abundance effects are nicely orthogonal. The effects of ADF width increase as the population ages. If we measure UV bump strength from farther in the UV and if we measure the metallicity from optical spectral indices, then it does indeed seem as if the narrow and normal widths can

be distinguished, with the only effect unaccounted for being dust extinction. We therefore tentatively judge that the prospects are bright for measuring the ADF width galaxies whose ages are fairly unimodal and whose dust content is characterized well. Using near-UV spectral indices as a proxy for photometric color would presumably lessen the effects of dust extinction and make the method more robust.

## 5 SUMMARY

Using the evolving Worthey models (Worthey 1994; Trager et al. 2008; Lee et al. 2009; Tang & Worthey 2013; Worthey et al. 2014b), we investigate composite stellar population models with different metallicity spreads. In integrated light, the narrower ADF appears more metal rich (“red lean”) and the disparity between narrow and wide ADFs widens as peak  $[M/H]$  move to a higher metallicity (“red spread”). Wide-width ADFs and the Simple Model ADF are ruled out because of the need for unreasonably large  $[M/H]$ <sup>6</sup>. Star by star, we confirm that the normal-width ADF replicates the observed solar neighborhood and MW bulge ADFs, and our modeling indicates that the normal-width or narrow-width ADF also fits elliptical galaxies in integrated light.

The good match of elliptical galaxy colors and TiO strengths with MW bulge templates (Terndrup et al. 1990) inspires us to find out if the MW bulge element abundance trend can be applied to elliptical galaxies. We model CSPs with MW bulge chemical compositions, tracking the detailed behavior of each element as a function of  $[M/H]$ , CSPs with scaled solar abundances, and CSPs with an elemental mixture chosen to match massive elliptical galaxies (Conroy et al. 2014), then compare model absorption feature indices with observed indices. Iron, Ti, and Mg vector about the same for the MW bulge and elliptical galaxies, while the trends of C, Na, and Ca are different. If the MW bulge is analogous to a low velocity dispersion elliptical galaxy, attempting to discern implications about elliptical galaxy evolution based on various nucleosynthetic processes associated with different environments (star formation timescales, galactic winds, stellar population IMF, supernova mass- and metallicity dependent yields, and white dwarf electron density) leads to no clear astrophysical frontrunner as to the cause of the abundance trends.

We perform an exercise to feed our MW bulge CSP models based on one set of stellar evolutionary isochrones into a chemical mixture inversion program based on a different set of stellar evolutionary isochrones and find that the parameters were recovered fairly well in the sense of matching the ADF-weighted mass average abundances. Our particular exercise uncovered a systematic trend toward younger ages. Elemental mixtures are recovered well, though in our case  $[N/Fe]$  came out on the low side, while  $[Ti/Fe]$  and  $[Si/Fe]$  were too high. The age and abundance systematics uncovered serve to urge further study of the inversion process.

We investigate whether the width of an ADF could be

<sup>6</sup> For additional discussion of the Simple Model ADF, see Worthey et al. (1996)

measured from integrated light alone, and find a successful technique: photometric colors of very long wavelength span. The main caveats for old stellar populations are dust content and the correct subtraction of whatever ultraviolet-bright subpopulation might be present.

## 6 ACKNOWLEDGEMENT

The authors wish to thank Washington State University and its Department of Physics and Astronomy, G. J. Graves, S. C. Trager, and J. Serven for the use of their data, and an anonymous referee for helpful comments. This research has made use of the VizieR catalogue access tool, CDS, Strasbourg, France.

## REFERENCES

- Alves-Brito, A., Meléndez, J., Asplund, M., Yong, D., 2010, *A&A*, 513, 35
- Arnett, W. D., 1971, *ApJ*, 166, 153
- Asplund, M., Grevesse, N., Sauval, A. J., Scott, P., 2009, *ARA&A*, 47, 481
- Babusiaux C., et al., 2010, *A&A*, 519, A77
- Bender, R., Burstein, D., Faber, S. M., 1993, *ApJ*, 411, 153
- Bensby, T., Feltzing, S., Lundström, I., 2003, *A&A*, 410, 527
- Bensby, T., et al., 2013, *A&A*, 549, 147
- Bensby, T., Feltzing, S., Oey, M. S., 2014, *A&A*, 562, A71
- Bertelli, G., Bressan, A., Chiosi, C., Fagotto, F., Nasi, E., 1994, *A&AS*, 106, 275
- Bertelli, G., Girardi, L., Marigo, P., Nasi, E., 2008, *A&A*, 484, 815
- Bertelli, G., Nasi, E., Girardi, L., Marigo, P., 2009, *A&A*, 508, 355
- Bruzual, A., G., Charlot, S., 1993, *ApJ*, 405, 538
- Bruzual, A. G., Charlot, S., 2003, *MNRAS*, 344, 1000
- Burstein, D., Faber, S. M., Gaskell, C. M., Krumm, N., 1984, *ApJ*, 287, 586
- Burbidge, E. M., Burbidge, G. R., Fowler, W. A., Hoyle, F., 1957, *Reviews of Modern Physics*, 29, 547
- Castelli, F., Gratton, R. G., Kurucz, R. L., 1997, *A&A*, 318, 841
- Chen, Y. Q., Nissen, P. E., Zhao, G., Zhang, H. W., Benoni, T., 2000, *A&A Supplement*, 141, 491
- Clayton, D., 2007, *Handbook of Isotopes in the Cosmos*, Cambridge, UK: Cambridge University Press
- Conroy, C., van Dokkum, P. G., Graves, G. J., 2013, *ApJ*, 763, 25
- Conroy, C., Graves, G. J., van Dokkum, P. G., 2014, *ApJ*, 780, 33
- Davies, R. L., Sadler, E. M., Peletier, R. F., 1993, *MNRAS*, 262, 650
- De, S., et al., 2014, *ApJ*, 787, 149
- Edvardsson, B., Andersen, J., Gustafsson, B., Lambert, D. L., Nissen, P. E., Tomkin, J., 1993, *A&A*, 275, 101
- Ekström, S., et al., 2012, *A&A*, 537, A146
- Frogel, J. A., Mould, J., Blanco, V. M., 1990, *ApJ*, 352, 96
- Fulbright, J. P., McWilliam, A., Rich, R. M., 2006, *ApJ*, 636, 821
- Fulbright, J. P., McWilliam, A., Rich, R. M., 2007, *ApJ*, 661, 1152
- Geisler, D., Smith, V. V., Wallerstein, G., Gonzalez, G., Charbonnel, C., 2005, *AJ*, 129, 1428
- Georgy, C. et al., 2013, *A&A*, 558, 103
- Girardi, L. et al., 2010, *ApJ*, 724, 1030
- Girardi, L., Marigo, P., Bressan, A., Rosenfield, P., 2013, *ApJ*, 777, 142
- González, J. J., 1993, Ph.D. thesis, Univ. California, Santa Cruz
- Graves, G. J., Faber, S. M., Schiavon, R. P., Yan, R., 2007, *ApJ*, 671, 243
- Grevesse, N., Sauval, A. J., 1998, *Space Sci. Rev.*, 85, 161
- Grevesse, N., Asplund, M., Sauval, A. J., 2007, *Space Sci. Rev.*, 130, 105
- Gustafsson, B., Edvardsson, B., Eriksson, K., Jørgensen, U. G., Nordlund, Å., Plez, B., 2008, *A&A*, 486, 951
- Haywood, M., 2001, *MNRAS*, 325, 1365
- Jeong, H., Yi, S. K., Kyeong, J., Sarzi, M., Sung, E., Oh, K., 2013, *ApJS*, 208, 7
- Johansson, J., Thomas, D., Maraston, C., 2012, *MNRAS*, 421, 1908
- Johnson, C. I., Rich, R. M., Kobayashi, C., Fulbright, J. P., 2012, *ApJ*, 749, 175
- Johnson, C. I., Rich, R. M., Kobayashi, C., Kunder, A., Pilachowski, C. A., Koch, A., de Propris, R., 2013, *ApJ*, 765, 157
- Jørgensen, B. R., 2000, *A&A*, 363, 947
- Kobayashi, C., Umeda, H., Nomoto, K., Tominaga, N., Ohkubo, T., 2006, *ApJ*, 653, 1145
- Kuntschner, H., et al., 2006, *MNRAS*, 369, 497
- La Barbera, F., Ferreras, I., Vazdekis, A., de la Rosa, I. G., de Carvalho, R. R., Trevisan, M., Falcón-Barroso, J., Ricciardelli, E., 2013, *MNRAS*, 433, 3017
- Lee, H., et al., 2009, *ApJ*, 694, 902
- Hill, V., et al., 2011, *A&A*, 534, A80
- MacArthur, L. A., González, J. J., Courteau, S., 2009, *MNRAS*, 395, 28
- Marigo, P., Girardi, L., Bressan, A., Groenewegen, M. A. T., Silva, L., Granato, G. L., 2008, *A&A*, 905, 883
- Meléndez, J., et al., 2008, *A&A*, 484, 21
- Mihalas, D., 1970, *Stellar Atmospheres, A Series of Books in Astronomy and Astrophysics*, San Francisco: Freeman
- Ness, M., et al., 2013, *MNRAS*, 430, 836
- Nomoto, K., Thielemann, F. K., Yokoi, K., 1984, *ApJ*, 286, 644
- Nomoto, K., Iwamoto, K., Nakasato, N., Thielemann, F. K., Brachwitz, F., Tsujimoto, T., Kubo, Y., Kishimoto, N., 1997, *Nuclear Physics A*, 621, 467
- Nomoto, K., Tominaga, N., Umeda, H., Kobayashi, C., Maeda, K., 2006, *Nuclear Physics A*, 777, 424
- Origlia, L., Rich, R. M., Castro, S., 2002, *AJ*, 123, 1559
- Ortolani, S., Renzini, A., Gilmozzi, R., Marconi, G., Barbay, B., Bica, E., Rich, R. M., 1995, *Nature*, 377, 701
- Pagel, B. E. J., 1997, *Nucleosynthesis and Chemical Evolution of Galaxies*, pp. 392. ISBN 0521550610. Cambridge, UK: Cambridge University Press, October 1997
- Pipino A., Matteucci F., 2004, *MNRAS*, 347, 968
- Pipino, A., Chiappini, C., Graves, G., Matteucci, F., 2009, *MNRAS*, 396, 1151
- Poole, V., Worthey, G., Lee, H. C., Serven, J., 2010, *AJ*, 139, 809

- Reddy, B. E., Lambert, D. L., Allende Prieto, C., 2006, MNRAS, 367, 1329
- Rich, R. M., Origlia, L., 2005, ApJ, 634, 1293
- Rich, R. M., Origlia, L., Valenti, E., 2007, ApJ, 665, 119
- Rich, R. M., Origlia, L., Valenti, E., 2012, ApJ, 746, 59
- Ryde, N. et al., 2010, A&A, 509, 20
- Saglia, R. P., Maraston, C., Thomas, D., Bender, R., Colless, M., 2002, ApJL, 579, L13
- Salpeter, E. E., 1955, ApJ, 121, 161
- Sánchez-Blázquez, P., Gorgas, J., Cardiel, N., González, J. J., 2006a, A&A, 457, 787
- Sánchez-Blázquez, et al., 2006b, MNRAS, 371, 703
- Santos, Jr., J. F. C., Frogel, J. A., 1997, ApJ, 479, 764
- Salaris, M., Weiss, A., Cassarà, L. P., Piovan, L., Chiosi, C., 2014, A&A, 565, 9
- Serven, J., 2010, Ph.D. thesis, Washington State Univ.
- Serven, J., Worthey, G., Briley, M. M., 2005, ApJ, 627, 754
- Serven, J., Worthey, G., 2010, AJ, 140, 152
- Shetrone, M. D., Côté, P., Sargent, W. L. W., 2001, ApJ, 548, 592
- Shetrone, M., Venn, K. A., Tolstoy, E., Primas, F., Hill, V., Kaufer, A., 2003, AJ, 125, 684
- Tang, B., Worthey, G., 2013, MNRAS, 429, 3174
- Terndrup, D. M., Frogel, J. A., Whitford, A. E., 1990, ApJ, 357, 453
- Thielemann, F. K., Nomoto, K., Yokoi, K., 1986, A&A, 158, 17
- Thomas, D., Johansson, J., Maraston, C., 2011, MNRAS, 412, 2199
- Timmes, F. X., Woosley, S. E., Weaver, T. A., 1995, ApJS, 98, 617
- Trager, S. C., Worthey, G., Faber, S. M., Burstein, D., González, J. J., 1998, ApJS, 116, 1
- Trager, S. C., Faber, S. M., Worthey, G., González, J. J., 2000, AJ, 120, 165
- Trager, S. C., Faber, S. M., Dressler, A., 2008, MNRAS, 386, 715
- Tremaine, S., et al., 2002, ApJ, 574, 740
- Valdes, F., Gupta, R., Rose, J. A., Singh, H. P., Bell, D. J., 2004, ApJS, 152, 251
- van den Hoek, L., Groenewegen, M., 1997, A&AS, 123, 305
- Wheeler, J. C., Sneden, C., Truran, J. W., Jr., 1989, ARA&A, 27, 279
- Woosley, S. E., Weaver, T. A., 1995, ApJS, 101, 181
- Woosley, Woosley, S. E., Heger, A., Weaver, T. A., 2002, Rev. Mod. Phys., 74, 1015
- Worthey, G., Faber, S. M., González, J. J., 1992, ApJ, 398, 69
- Worthey, G., 1994, ApJS, 95, 107
- Worthey, G., Faber, S. M., González, J. J., Burstein, D., 1994, ApJS, 94, 687
- Worthey, G., Dorman, B., Jones, L. A., 1996, AJ, 112, 948
- Worthey, G., 1998, PASP, 110, 888
- Worthey, G., Mateo, M., Alonso-García, J., España, A. L., 2004, PASP, 116, 295
- Worthey, G., España, A., MacArthur, L. A., Courteau, S., 2005, ApJ, 2005, 631, 820
- Worthey, G., Ingermann, B. A., Serven, J., 2011, ApJ, 729, 148
- Worthey, G., Tang, B., Serven, J., 2014a, ApJ, 783, 20
- Worthey, G., Danilet, A. B., Faber, S. M., 2014b, A&A, 561, A36
- Wyse, R. F. G., Gilmore, G., 1995, AJ, 110, 2771
- Zoccali, M., et al., 2003, A&A, 399, 931
- Zoccali, M., Hill, V., Lecureur, A., Barbuy, B., Renzini, A., Minniti, D., Gómez, A., Ortolani, S., 2008, A&A, 486, 177